NANO LETTERS

Letter

pubs.acs.org/NanoLett

High-Performance Multipanel Biosensors Based on a Selective Integration of Nanographite Petals

Irene Taurino,*[,†] Arnaud Magrez,[‡] Federico Matteini,[§] Andrea Cavallini,[†] László Forró,[∥] Giovanni De Micheli,[†] and Sandro Carrara[†]

[†]Laboratory of Integrated Systems, [‡]Crystal Growth Facility, [§]Laboratory of Semiconductor Materials, and [∥]Laboratory of Physics of Complex Matter, EPFL - École Polytechnique Fédérale de Lausanne, Lausanne, Switzerland

ABSTRACT: We report the first selective growth of nanographite petals and various carbon nanomaterials onto a multipanel electrochemical platform. Different types of nanomaterials can be obtained by fine-tuning the growth parameters of the chemical vapor deposition (CVD) process. First, absolute novelty is the catalytic CVD selective growth of different carbon nanomaterials only on the working electrodes of the platform. A second novelty is the growth obtained at complementary metal−oxide−semiconductor compatible temperatures. These novel electrodes have been incorporated in sensors in which performance characteristics improve with the content of nanostructures. Unprecedented sensing parameters with respect to both direct and enzyme-mediated electrochemical biodetection have been obtained.

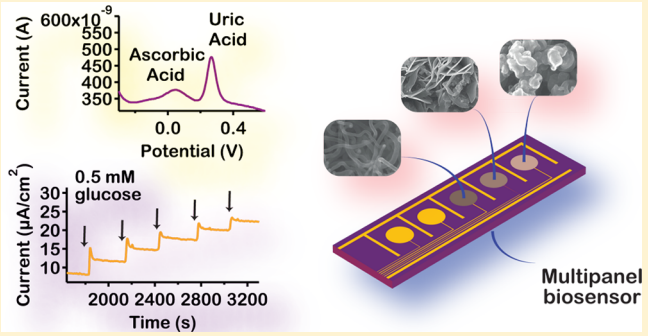

KEYWORDS: *Carbon nanomaterials, microelectrode nanostructuration, CVD, CMOS compatible temperatures, electrochemical multipanel biosensor*

The simultaneous detection of endogenous and exogenous biocompounds is critically important for diagnostics, disease treatments, health control, and prevention.[1−3] Electrochemical devices based on array of sensing sites at the microscale are particularly useful to detect more than one substance at a time.[4] Recently, carbon nanomaterials were employed to enable the detection of molecules either in the normal and pathological concentration ranges that are relevant for clinical studies.[5−7] The development of tailored integration methods to nanostructure microsurfaces is quite challenging. The most used techniques (electropolymerization and drop casting) suffer from scarce reproducibility, long preparation, expensive instrumentation, and decrease of the device performance. The reduction of the sensing performance is due to the presence of binders that hinder the nanomaterial properties, making the nanostructuration unstable in aqueous environment.[8]

The direct synthesis is the principal approach to place carbon nanostructures on an electrode and producing a close contact between the nanomaterials and the underlying metal substrate. Unfortunately, this method presents several limitations: the tendency of some classes of carbon nanomaterials to grow on dielectric layers complicates their selective positioning on metal surfaces; their growth onto the passivation layer of the device creates short circuits among electrodes of the platform making the multipanel detection impossible. The interdiffusion and the alloying between the catalyst and the metal electrode surface prevent the nanocarbon formation at the chemical vapor deposition (CVD) temperatures.[9] Nevertheless, the possibility to fabricate nanomaterials directly on metal is of crucial importance to obtain biosensors with improved features.[10] Finally, the CVD temperatures are too high (650−1200 °C) for the direct integration of nanomaterials with the front-end complementary metal−oxide−semiconductor (CMOS) architectures.[11]

Here, we propose an innovative approach to selectively grow carbon nanomaterials on Pt microelectrodes of a biosensor array down to CMOS temperatures. We used electrodeposition as a promising and versatile method that grants the easy tuning of the catalyst's thickness and morphology. By modifying such catalyst properties, we were able to selectively synthesize different amounts of nanographite, nanotubes, and their hybrids. The following method also enabled the growth of graphitic nanopetals at 450 °C. The formation of such structures by CVD represents a completely new approach. We reached excellent sensing parameters by both direct detection of highly electroactive metabolites and sensing mediated by an enzyme. To fabricate the biosensor standard photolithography and lift-off processes were used. The materials were accurately selected to be resistant at the high growth temperatures. For instance, HfO_2, produced by atomic layer deposition, was chosen as passivation layer because of its good adhesion to the underlayer material.

Received: February 7, 2014
Revised: April 14, 2014
Published: May 6, 2014

After the sensor microfabrication (Figure 1a-i,a-ii), Fe_2Co was electrodeposited on the Pt working electrodes (WEs) of

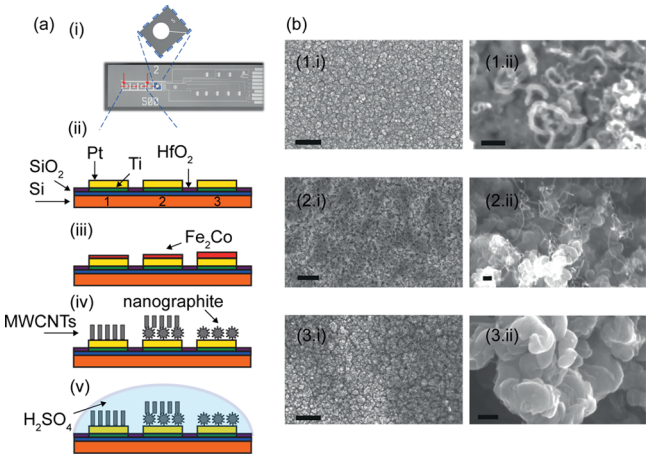

Figure 1. (a) Top view of the microelectrode array layout (i) and schematic of the cross section (ii). Nanointegration steps of the array-based biosensor: electrodeposited Fe_2Co layers with increased thickness (iii), MWCNTs, hybrid MWCNT-nanographite and nanographite growths (iv), and chemical activation (v). (b) SEM images of Fe_2Co coatings obtained after applying a voltage of −1.4 V for 4 s (1.i), 15 s (2.i) and 30 s (3.i) (bars, 1 μm) and respective growths (MWCNTs (1.ii), hybrid MWCNTs-nanographite (2.ii) and nanographite (3.ii) (bars, 100 nm)).

the device (Figure 1a-iii) starting from sulfate solutions (Fe−Co concentration ratio in solution was 2:1). Layers of Fe_2Co were grown on each WE via electrodeposition. Such technique has the advantage to be versatile, fast, and compatible with the microfabricated platform. Moreover, thicker films can be obtained simply prolonging the time of applied voltage.

Five minutes of carbon flow in the quartz tube led to the formation of nanographite, MWCNTs, and hybrid multiwalled carbon nanotubes (MWCNTs)−nanographite (Figure 1a-iv) depending on the nature of the catalyst coating. To increase the electroactivity of the nanostructures carbon nanomaterials were chemically treated in sulfuric acid before any measurement (Figure 1a-v).

The growth of carbon nanomaterials on metals usually employs a dielectric buffer layer between the catalyst and the substrate.[12] Unfortunately, this configuration is detrimental for the performance, because it creates a barrier in the electrical connection. In this work, the catalyst was directly electrodeposited on the Pt electrodes in order to ensure a good electric coupling. The layer maintained its catalytic activity during the catalytic CVD process.

Figure 1b shows scanning electron microscopy (SEM) images of catalyst coatings produced by increasing the deposition time (1−3.i). The respective carbon growths (1−3.ii) were obtained at 600 °C. As the Fe_2Co thickness increases (rate of the thickness increase is of about 21.6 ± 1.8 nm/s), the amount of MWCNTs decreases and nanographite simultaneously starts to be produced. The highest carbon yield was obtained from thicker catalyst layers. Direct synthesis of nanomaterials has been successfully accomplished on specific sites of the sensing platform. Thicker catalyst layers produce MWCNTs with larger diameters as long as no nanographite is formed onto the electrode (yellow bars in Figure 2a). The synthesis of nanographite starts from thinner catalyst layers at

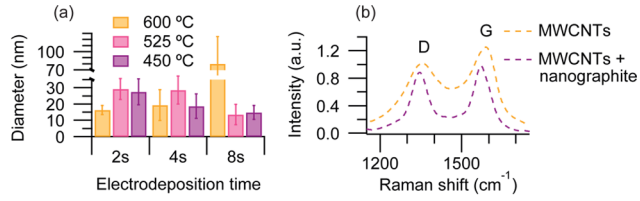

(c)

I_d/I_g	1.7 ± 0.2	1.5 ± 0.1
$I_{g'}/I_g$	6.8 ± 1.5	1.3 ± 0.2
I_g/I_d	4.0 ± 0.9	0.9 ± 0.1
D (cm^{-1})	1352.0 ± 1.3	1349.0 ± 1.4
G (cm^{-1})	1599.7 ± 0.8	1585.9 ± 1.9
G' (cm^{-1})	2678.1 ± 2.4	2698.3 ± 1.0
FWHM(D)	109.1 ± 9.7	99.0 ± 3.6
FWHM(G)	63.8 ± 4.4	76.2 ± 0.2
FWHM(G')	267.1 ± 23.9	116.4 ± 9.3

Figure 2. (a) Diameter distribution of MWCNTs grown from Fe_2Co with different thickness and produced at 600, 525, and 450 °C. In absence of the nanographite in the sample, the MWCNT diameter increases with the catalyst thickness (rate of the thickness increase: 21.6 ± 1.8 nm/s). Conversely, if nanographite is produced, the MWCNT diameter decreases. (b) D and G peaks related to MWCNTs and MWCNTs/nanographite produced at 600 °C. (c) Values of I_d/I_g, $I_{g'}/I_g$, $I_{g'}/I_d$, D, G and G′ positions and FWHM of MWCNTs and MWCNTs/nanographite produced at 525 °C from catalyst layers deposited for 2 and 8 s (average thickness of 54 ± 6 nm and 112 ± 14 nm, respectively; bars: 100 nm).

temperatures lower than 600 °C and once graphite grows onto the Pt surfaces, the MWCNT diameters drastically decreases (pink and violet bars in Figure 2a).

Raman spectra reveal much about the nature of the produced nanomaterials. Figure 2b shows an example of the D and G peaks of MWCNTs and hybrid MWCNTs/nanographite. SEM images in Figure 2 clearly show that the amount of nanographite increases as the thickness of the catalyst coating becomes higher. As expected, the presence of nanographite determines the shift of the G and D bands toward lower values and of G′ peak toward higher values, the decrease of the I_d/I_g, $I_{g'}/I_g$, $I_{g'}/I_d$ ratios and sharper G′ peaks in accordance with the literature.[13] Peak ratios, peak positions, and values of the full width at half-maximum (FWHM) are reported in Figure 2c.

We succeeded in fabricating CNTs and nanographite down to 450 °C, a temperature that makes it possible to grow nanomaterials directly onto the front-end of CMOS data acquisition circuits. Generally, only amorphous carbon grows below 600 °C when a CVD system based on thermal decomposition of C_2H_2 is used. In this work, the oxidative dehydrogenation reaction of CO_2 and C_2H_2[14] was proven to improve the activity and the lifetime of the catalyst on metallic microsurfaces resulting in nanocarbon growths also at low temperatures. We noted a decrease of carbon yield by lowering the synthesis temperature but we successfully obtained a high yield of carbon nanomaterials that are of crucial importance for improved sensing performance also at CMOS compatible temperatures. More precisely, after the first synthesis, we covered the already grown nanomaterials with a further thin

dx.doi.org/10.1021/nl500493m | Nano Lett. 2014, 14, 3180−3184

layer of catalyst. Then, a second synthesis was carried out at 450 °C under the same growth conditions. The amount of CNTs effectively increases (Figure 3). In addition, the new

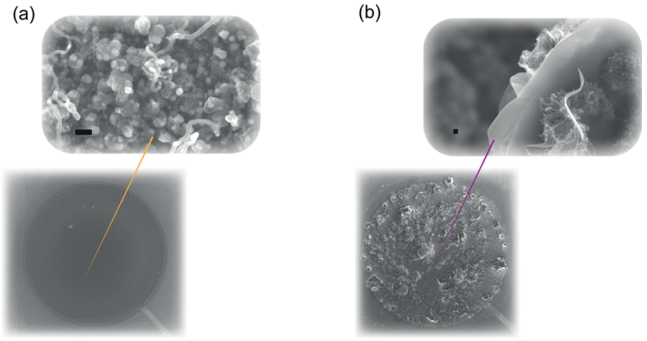

Figure 3. SEM images of carbon nanomaterials grown at 450 °C after the first deposition on 4 s of electrodeposited Fe_2Co layer (i) and after the second CVD synthesis onto the same already nanostructured electrode covered with 2 s of electrodeposited catalyst (ii). Bars: 100 nm.

catalyst surface catalyzed the formation of very thin graphitic petals. Figure 3b shows these nanostructures with MWCNTs inserted in between them. To the best of our knowledge, this is the first experimental demonstration of such a kind of carbon nanopetals grown by a catalytic CVD process. Other authors have produced similar nanostructures but mainly by plasma CVD synthesis.[15] Interestingly, carbon nanopetals were obtained at CMOS compatible temperatures.

We characterized some of the nanostructured microelectrodes before and after the acid activation. The increase of capacitive and of faradic current (Figure 4a,b), more evident when the electrode is covered with a largest amount of nanomaterials, demonstrates the efficiency of this treatment in forming defects and functional groups[16] and in making more powerful the sensing. For hybrid MWCNTs/nanographite grown at 600 °C, the total capacitance is 89 and 524 nF before and after the treatment, respectively. Hybrid MWCNTs/nanographite grown at 525 °C shows lower yield and, consequently, a smaller increase of the capacitance (21 and 67 nF before and after the activation, respectively). This activation step is very important also because it increases the number of electrocatalytic sites enabling an efficient immobilization of proteins.[17]

To investigate the electrochemical behavior of the nanostructured electrodes, we measured different concentrations of uric acid (UA) that was selected as examples of electroactive metabolite of significant importance in biosensing. Figure 4c shows the improvement of the sensing parameters with the yield of the deposited carbon nanomaterials. Hybrid nanomaterials grown at 600 °C with the highest yield and consequently the largest surface area have shown the best sensing properties. In particular, UA concentrates at electrodes based on carbon nanomaterials by hydrophobic interactions. The hydrophobicity of electrodes modified with directly grown carbon nanomaterials is higher than that of electrodes nanostructured by other methods. We carried out only a mild activation after the carbon nanomaterial synthesis. On the other hand, carbon nanostructures, especially CNTs, which are incorporated onto electrodes by more conventional approaches, usually have a large amount of hydrophilic sites (functional groups) because of the extensive treatments preceding their use. The strong

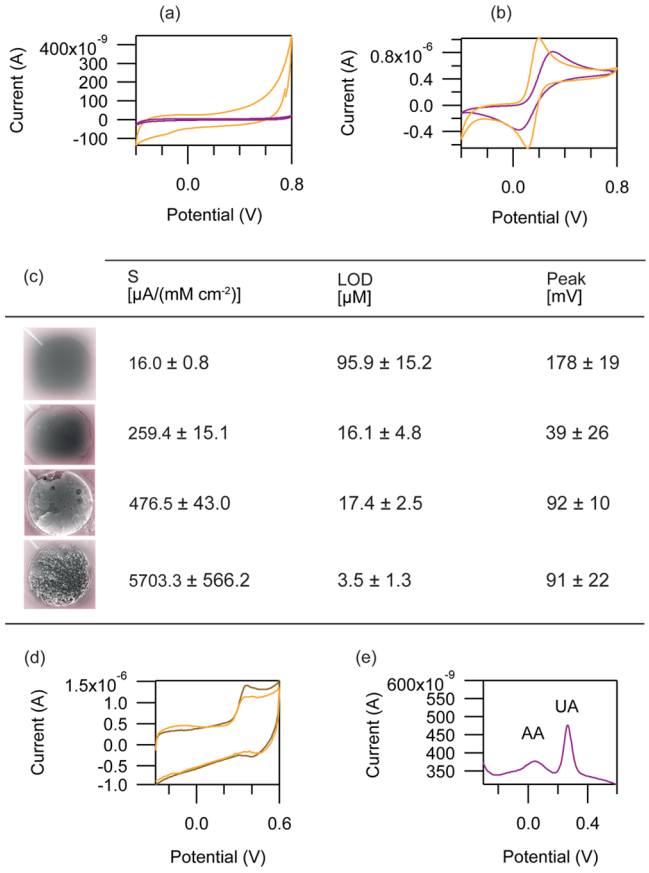

Figure 4. CVs of Pt nanostructured with hybrid MWCNTs/nanographite grown at 525 °C from 8 s of electrodeposited catalyst (a) in phosphate buffered saline (PBS) solution (10 mM; pH 7.4) and (b) in 2.5 mM $K_3[Fe(CN)_6]$/PBS (10 mM; pH 7.4) solution. The violet and yellow lines refer to the nanomaterial's response before and after the chemical activation in 6 M sulfuric acid, respectively. Potential window: −0.4/+0.8 V. Scan rate: 0.05 V/s. The effect of the treatment is evident from the increase of the background current and the efficiency for sensing from the increase of the peak response. (c) The sensitivity (S), the detection limit (LOD), and the peak position obtained by detecting UA. We used bare electrodes, electrodes with MWCNTs, and with MWCNTs−nanographite grown at 525 and at 600 °C. (d) CVs with nanographite-modified electrode in human serum containing 25 μM (yellow line) and 100 μM (brown line) UA (scan rate: 0.02 V/s). (e) Discrimination of UA and AA by differential pulsed voltammetry with the nanostructured electrodes (scan rate: 0.01 V/s).

interaction UA-CVD grown carbon nanomaterials explains the high sensitivities we obtained. The oxidative peak shifts toward less positive values, which entails less power consumption (from ∼200 to ∼30−100 mV). Preliminary measurements in serum, carried out by using high yield nanographite-based electrodes, showed the presence of a clear peak. Figure 4d illustrates two cyclic voltammetries (CVs) obtained at different concentrations of UA diluted in human serum. The peak shift toward more positive potential (∼360 mV) in the real sample than in the synthetic one (∼90 mV). Bigger molecules in serum interact with the UA and reduce the electron transfer kinetics. No defined peak appeared by using bare electrodes. The nanostructured devices discriminate UA from ascorbic acid (AA), a well-known interfering compound (Figure 4e). The introduction of AA causes the shift of the UA peaks toward more positive potentials of ∼200 mV (peak position: +42 mV

dx.doi.org/10.1021/nl500493m | Nano Lett. 2014, 14, 3180−3184

for AA, +265 mV for UA). Also in this case, no defined peak is present if the bare electrode is used.

Additionally, an enzyme-mediated detection was proven to be dependent on the amount of material grown onto the electrode. Figure 5a shows an increased current response for

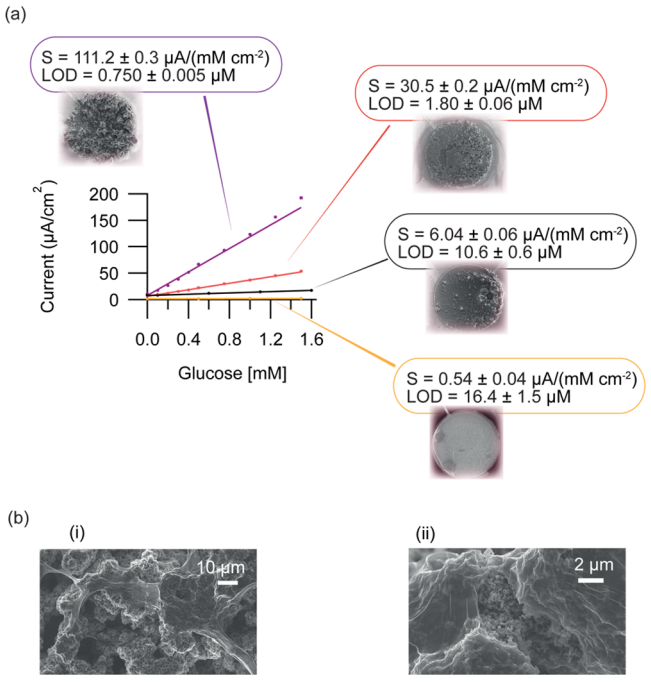

Figure 5. (a) Calibration curves for glucose detection of enzyme-based microelectrodes modified with an increased amount of carbon nanomaterials, respective SEM images and sensing parameters. (b) SEM images at lower (i) and higher (ii) magnification of nanographite-glucose oxidase modified microelectrode.

high yield nanostructured electrodes. In particular, we obtained the highest response using the most packed nanographite produced at 600 °C. The sensitivity and the detection limit were 111.2 ± 0.3 μA/(mM cm^2) and 745 ± 5 nM, respectively. These sensing parameters are superior compared to those found with other nanostructuration approaches.[18] The large surface area of the high-yield carbon nanomaterial-based electrodes favors the adsorption of a huge amount of glucose oxidase thus improving the sensitivity of the enzyme-mediated glucose detection. Figure 5b shows the presence of the adsorbed enzyme that seems to glue the nanomaterials. The diameter of MWCNTs increases from 22.6 ± 2.7 to 34.3 ± 17.1 nm. This finding confirms previous computations[19] proving that each MWCNT and nanographite fragment is surrounded by a single enzyme layer.

It is well-know that electrode fouling in real biosample is an issue for reproducible and accurate measurements. Taking that into account, we studied the fouling of the nanostructured electrodes.[20] We initially recorded multiple CVs in solutions containing 2.5 mM $K_3[Fe(CN)_6]$/PBS (10 mM, pH 7.4). The nanostructured Pt microelectrodes were then inserted for 10 min in a cell culture medium containing a wide range of biocompounds. An attenuation of the electroanalytical response was expected because of possible adsorption of biomolecules either on the polar sp^2 carbon created after the treatment and by hydrophobic interactions. The electrodes were then removed from the biosample, reinserted in the initial solution containing $K_3[Fe(CN)_6]$, and multiple CVs were recorded again. The reduction of the peak currents ranged between 16 and 26% and the increase of the peak-to-peak separation ranged between 29 and 164 mV. The highest fouling characterized the electrodes with low-yield carbon nanomaterials. Then, the procedure was repeated by keeping the electrodes in the cell medium for extra 45 and 60 min and both peak heights and potential positions unchanged for samples fully covered with nanomaterials.

In summary, we selectively grew nanographite, MWCNTs, and their hybrids onto an array of microelectrodes of an electrochemical biosensor. An accurate control of the CNT diameter, of the kind of nanomaterials, and of the carbon yield was possible by changing the thickness of the catalyst and the growth temperatures. Carbon growths were obtained down to temperatures compatible with CMOS circuits (450 °C). The carbon yield at low temperatures was increased by implementing two successive depositions. Thin graphitic nanopetals were synthesized for the fist time by a CVD system on top of nanostructures deposited at the first stage. The obtained nanostructured microelectrodes were proven to be powerful and competitive to sense different metabolites. By detecting UA, the sensitivity of the nanostructured microelectrodes was improved by 2 orders of magnitude from 16.0 ± 0.8 to 5703.3 ± 566.2 μA/(mM cm^2) than using bare electrodes. The limit of detection went down to some micromoles and the oxidation potential was significantly reduced, which means advantages in circuit design. The described nanostructuration approach allows us to discriminate UA from its very well-known interfering compound, the ascorbic acid, and to identify the UA peak in human serum. The enzyme-mediated detection of glucose showed a detection limit of some hundreds of nanomolars, one of the best ever found in literature.[18] It is worth noting that the fully nanostructured electrodes were not exposed to further degradation after the first minutes in cell medium. Moreover, the described nanostructured electrochemical device paves the way for using nanostructured sensing sites at the microscale on unique multipanel platforms highly integrated on the front-end electronics.

Methods. *Device Fabrication.* Devices were produced on Si wafers with 500 nm of Si oxide. First, 200 nm of Pt were deposited by evaporation (Alcatel EVA 600). To improve the adhesion, 20 nm of Ti were added between Pt and Si oxide. After the lift-off, HfO_2 (20 nm) was deposited via atomic layer deposition (BENEQ TFS200). Then, patterns of electrodes and respective contacts were introduced on the insulating material. A selective removal of HfO_2 was realized by dry etching (Alcatel AMS 200 DSE, 90 s). Finally, the wafer was diced in single devices. Each device includes five working electrodes (WEs) with a diameter of 564 μm that share the same counter and reference electrode.

Catalyst Electrodeposition. The solutions used for the deposition of Fe_2Co layers were mixtures of 0.2 M $FeSO_4{\cdot}H_2O$ and 0.1 M $CoSO_4{\cdot}H_2O$ (BioChemica, AppliChem). The supporting electrolyte contained NaCl (0.5 M, Sigma) and H_3BO_3 (0.5 M, BioChemica, AppliChem). Electrodeposition was carried out by applying −1.4 V (room temperature; solution stirred at 90 rpm). Pt (area = 12.56 mm^2) was used as counter electrode and placed in parallel to the working electrode. A Ag electrode was used as reference. All the experiments were carried out using an Autolab potentiostat under a computerized control. Catalyst coatings with different thickness were electrodeposited onto the microelectrodes of the device by varying the interval of the applied potential (from

dx.doi.org/10.1021/nl500493m | Nano Lett. 2014, 14, 3180−3184

2 to 30 s). Thicknesses were measured with a Dektak XT Profilometer (Bruker). To evaluate the rate of thickness increase with the electrodeposition time, we prepared three samples per each deposition time (2, 8, 15, and 30 s). For each sample, measurements were taken in triplicate. The thickness showed a linear increase with the electrodeposition time (R^2 = 0.99).

Carbon Nanomaterials Synthesis. Nanographite, hybrid MWCNTs−nanographite, MWCNTs, and thin graphitic nanopetals were synthesized using a catalytic CVD system.[14] The devices were heated to the growth temperature under Ar (60 l/h) and H_2 flow for some minutes (3 or 10 min). Then, carbon precursors (C_2H_2 and CO_2; flow rate, 0.25 l/h per each; Ar flow rate, 45 l/h) fed the quartz tube for 5 min. Furnace temperatures ranged between 600 and 450 °C. Before the furnace was opened, Ar was introduced for 10 min at 60 l/h.

Growths Characterization. Chemical composition and morphology of the catalyst and morphology of the carbon-coated electrodes were examined by high-resolution scanning microscopy (Zeiss MERLIN). The CNT diameters were calculated by using an ImageJ software.[21] Raman spectra were acquired using a homemade micro-Raman microscope.[22] A triple grating spectrometer (TriVista 555) was used to analyze the spectra. The laser (wavelength: 488 nm) was focused on a diffraction-limited spot of around 0.65 μm^2 until reaching a power density of 2.2−2.3 mW/μm^2. The time of acquisition varied from 2 to 5 min. The fitting of the Raman modes was realized with IgorPro software (Wavemetrics, Lake Oswego, OR, USA) by using Lorentzians.[13]

Electrochemical Measurements. Before the measurements, the nanostructured electrodes were treated in H_2SO_4 (Sigma) solution (6 M) for 5−6 h.[23] Electrochemical experiments were performed in PBS (10 mM, pH 7.4, Sigma) using the three Pt electrode configuration of the device under aerobic conditions. All the measurements were conducted with Autolab potentiostat controlled by Nova software. We used IgorPro software for the data analysis. UA and human serum were purchased from Sigma and VWR, respectively. Electrodes were modified with glucose oxidase from Roche by physical adsorption. A solution of the enzyme was freshly prepared (concentration: 15 mg/mL) and 1 μL was cast onto the electrodes and kept overnight at 4 °C. A H_3BO_3 buffer solution (0.02 M; pH 9.0 at 25 °C) was employed to prepare 3.57 mM UA stock solution. It was freshly prepared before each measurement. All the dilutions were carried out in PBS (10 mM, pH 7.4) solution. The solution of glucose was prepared at least the day before the measurements and stored in the fridge at 4 °C. To study the electrode fouling in biosample, we used a Dulbecco's Modified Eagle Medium from Gibco/Life Technologies.

AUTHOR INFORMATION

Notes

The authors declare no competing financial interest.

ACKNOWLEDGMENTS

The authors thank Anna Fontcuberta i Morral for the Raman setup and Laurent Bernard for the preparation of the CVD system. The research was supported by the i-IronIC project. The i-IronIC project was financed by a grant from the Swiss Nano-Tera.ch initiative and evaluated by the Swiss National Science Foundation. The work performed at the LPMC and Crystal Growth Facility is supported by the European Commission (FP7, Marie-Curie ITN NAMASEN). F.M. acknowledges financial support from ERC Grant UpCon.

REFERENCES

(1) McNerney, R.; Daley, P. *Nat. Rev. Microbiol.* **2011**, *9*, 204−213.
(2) Carrara, S.; Cavallini, A.; Erokhin, V.; Micheli, G. D. *Biosens. Bioelectron.* **2011**, *26*, 3914−3919.
(3) Carrara, S.; Shumyantseva, V. V.; Archakov, A. I.; Samor, B. *Biosens. Bioelectron.* **2008**, *24*, 148−150.
(4) Wang, J. *Biosens. Bioelectron.* **2006**, *21*, 1887−1892.
(5) Krauss, T. D. *Nat. Nanotechnol.* **2009**, *4*, 85−86.
(6) Taurino, I.; Reiss, R.; Richter, M.; Fairhead, M.; Thny-Meyer, L.; Micheli, G. D.; Carrara, S. *Electrochim. Acta* **2013**, *93*, 72−79.
(7) Lin, Y.; Lu, F.; Tu, Y.; Ren, Z. *Nano Lett.* **2004**, *4*, 191−195.
(8) Hoyt, A. E.; Ricco, A. J.; Bartholomew, J. W.; Osbourn, G. C. *Anal. Chem.* **1998**, *70*, 2137−2145.
(9) Nessim, G. D.; Seita, M.; OBrien, K. P.; Hart, A. J.; Bonaparte, R. K.; Mitchell, R. R.; Thompson, C. V. *Nano Lett.* **2009**, *9*, 3398−3405.
(10) Nessim, G. D.; Acquaviva, D.; Seita, M.; O'Brien, K. P.; Thompson, C. V. *Adv. Funct. Mater.* **2010**, *20*, 1306−1312.
(11) Jousseaume, V.; Cuzzocrea, J.; Bernier, N.; Renard, V. T. *Appl. Phys. Lett.* **2011**, *98*, 123103.
(12) Park, S.; Dong-Won, P.; Yang, C.-S.; Kim, K.-R.; Kwak, J.-H.; So, H.-M.; Ahn, C. W.; Kim, B. S.; Chang, H.; Lee, J.-O. *ACS Nano* **2011**, *5*, 7061−7068.
(13) Sadezky, A.; Muckenhuber, H.; Grothe, H.; Niessner, R.; Pöschl, U. *Carbon* **2005**, *43*, 1731−1742.
(14) Magrez, A.; Seo, J.; Smajda, R.; Korbely, B.; Andresen, J.; Mionić, M.; Casimirius, S.; Forró, L. *ACS Nano* **2010**, *4*, 3702−3708.
(15) Wu, Y.; Yang, B.; Zong, B.; Sun, H.; Shen, Z.; Feng, Y. *J. Mater. Chem.* **2004**, *14*, 469−477.
(16) Holloway, A. F.; Wildgoose, G. G.; Compton, R. G.; Shao, L.; Green, M. L. *J. Solid State Electrochem.* **2008**, *12*, 1337−1348.
(17) Lin, Y.; Taylor, S.; Li, H.; Fernando, K. S.; Qu, L.; Wang, W.; Gu, L.; Zhou, B.; Sun, Y.-P. *J. Mater. Chem.* **2004**, *14*, 527−541.
(18) Chen, C.; Xie, Q.; Yang, D.; Xiao, H.; Fu, Y.; Tan, Y.; Yao, S. *RSC Adv.* **2013**, *3*, 4473−4491.
(19) Boero, C.; Carrara, S.; Del Vecchio, G.; Calzà, L.; De Micheli, G. *Sens. Actuators, B* **2011**, *157*, 216−224.
(20) Park, J.; Show, Y.; Quaiserova, V.; Galligan, J. J.; Fink, G. D.; Swain, G. M. *J. Electroanal. Chem.* **2005**, *583*, 56−68.
(21) Rasband, W. *Image J*; U.S. National Institutes of Health: Bethesda, MD, 1997−2011; http://imagej.nih.gov/ij/ (accessed 2011-05-09).
(22) Ketterer, B.; Heiss, M.; Uccelli, E.; Arbiol, J.; Fontcuberta i Morral, A. *ACS Nano* **2011**, *5*, 7585−7592.
(23) Chen, Y.; Huang, J.; Chuang, C. *Carbon* **2009**, *47*, 3106−3112.